Structure–activity relationship for chelating phosphite ligands used in rhodium-catalyzed hydroformylations

Rocco Paciello [*], Lorenz Siggel [1], Heinz-Josef Kneuper, Nigel Walker, Michael Röper

BASF, 67056 Ludwigshafen, Germany

Received 10 March 1998; accepted 8 September 1998

Abstract

A simplified kinetic model was developed for the rhodium-catalyzed low-pressure hydroformylation using chelating phosphite ligands. This allowed the determination of the relative rate constants for linear and branched aldehyde formation starting with terminal olefins using data from complex product mixtures. Structural data were obtained using X-ray crystallography and served as the basis for molecular modeling of rhodium complexes with such chelating ligands. The interaction of linear and branched alkyl groups with the ligand environment in such complexes was quantified using molecular modeling. The energy differences obtained with molecular modeling were plotted against the energy differences obtained from kinetic experiments and a linear correlation was found. This type of approach, i.e., development of a structure–activity relationship, can be used to quickly and efficiently investigate such catalytic systems. © 1999 Elsevier Science B.V. All rights reserved.

Keywords: Hydroformylation; Rhodium; Phosphite ligand; Structure–activity relationship

1. Introduction

The hydroformylation of propylene to *n*- and *i*-butyraldehyde is one of the most important homogeneously catalyzed industrial processes. *n*-Butyraldehyde is a precursor for 2-ethyl-hexanol, an important plasticizer alcohol, and for *n*-butanol, a solvent and itself a precursor for further derivatives such as *n*-butylacetate and *n*-butylacrylate [1]. As these products account for the bulk of the present industrial demand, continuous efforts have been made to improve the selectivity of this process. [2]

Rhodium-catalyzed hydroformylations have achieved a dominant position for lower olefins such as propylene due to their excellent chemo- and regioselectivities, and due to the significant technical advantages offered by low-pressure processes. Although reactions of rhodium car-

---

[*] Corresponding author. E-mail: rocco.paciello@basf-ag.de

[1] E-mail: lorenz.siggel@zx.basf-ag.de.

[2] The demand for derivatives of *i*-butyraldehyde, e.g., isobutanol and its derivatives or condensation products such as neopentylglycol, has historically been much smaller. These products, however, have their uses. The selectivity of technical catalysts often has to be matched to the demands of a given product portfolio.
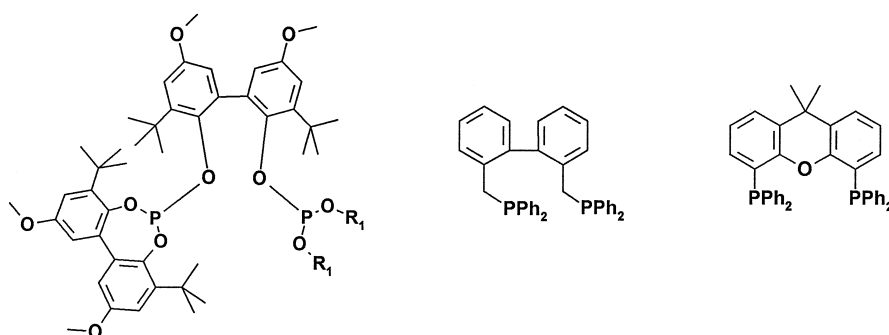
Fig. 1. Structures of selected chelating ligands.

bonyl complexes modified by triarylphosphines such as triphenylphosphine in the organic phase or, to a much lesser extent, sulfonated triphenylphosphine in the aqueous phase have been the mainstay of previous technical processes (for a recent review with a discussion of technical processes, see Ref. [2]), highly selective chelating ligands (Fig. 1), such as bisphosphines [3–6] and sterically hindered bisphosphites [7–11], have awakened considerable interest in recent years.

One of our projects in the Ammonia Laboratory, one of the central laboratories of BASF, concerns itself with the rational design of homogeneous transition metal catalysts. We have developed several tools, such as kinetic and molecular modeling, for this purpose and wish to present a part of this work in the following manuscript using chelating phosphite ligands as examples of highly selective catalysts for low-pressure rhodium-catalyzed hydroformylations.

2. Experimental

2.1. Ligand synthesis

The ligands used were synthesized as described in the literature [7,12], and characterized before use with the help of elemental analysis, NMR (^{31}P, ^{13}C, ^{1}H), melting point and mass spectroscopy.
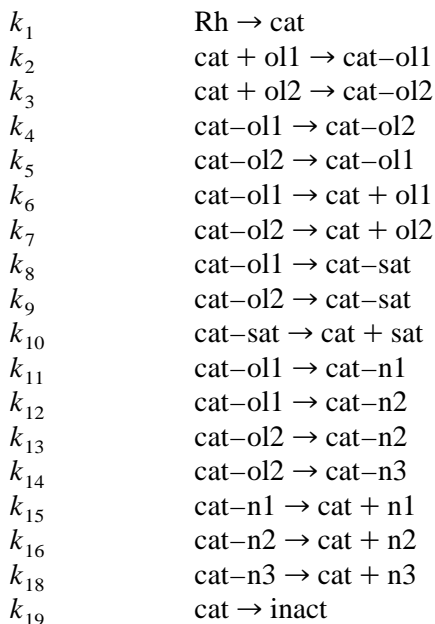
2.2. Kinetic experiments (general procedure)

A mechanically stirred 0.35-l autoclave (material: HC) outfitted with a gas dispersion turbine (standard tests, such as variation of the stirrer speed, show that gas transport under the experimental conditions is not diffusion limited) was filled with 160 g 1-octene (1.45 mol; freshly distilled), 120 g toluene and the appropriate amount of phosphorus ligand (the molar ratio of ligand to rhodium was held constant at 5). The autoclave was closed and flushed with a mixture of 50 vol% CO and 50 vol% H_2. This was accomplished by pressing up to 7 bar and releasing the pressure three times. The autoclave was then heated to 100°C and 0.15 g $Rh(CO)_2(acac)$ (0.58 mmol; acac = acetylacetonate) dissolved in 26 g of toluene were added to the reaction mixture. The reactions were run for a total of 90 min. Samples were taken at 5-min intervals the first 30 min and at 10-min intervals thereafter. The samples were quenched to 0°C, flushed with argon and immediately analyzed using a capillary GC (30 m OV-1 column, internal standard and correction factors). Remeasurement of the first samples showed that no changes occurred during time necessary to analyze the total run.

2.3. Kinetic modeling

In the kinetic modeling program used, all steps were approximated with first order rate

constants and varied using a multiparameter Gear iterator until the best fit was achieved. [3] The following model was used:

k_1	$Rh \rightarrow cat$
k_2	$cat + ol1 \rightarrow cat-ol1$
k_3	$cat + ol2 \rightarrow cat-ol2$
k_4	$cat-ol1 \rightarrow cat-ol2$
k_5	$cat-ol2 \rightarrow cat-ol1$
k_6	$cat-ol1 \rightarrow cat + ol1$
k_7	$cat-ol2 \rightarrow cat + ol2$
k_8	$cat-ol1 \rightarrow cat-sat$
k_9	$cat-ol2 \rightarrow cat-sat$
k_{10}	$cat-sat \rightarrow cat + sat$
k_{11}	$cat-ol1 \rightarrow cat-n1$
k_{12}	$cat-ol1 \rightarrow cat-n2$
k_{13}	$cat-ol2 \rightarrow cat-n2$
k_{14}	$cat-ol2 \rightarrow cat-n3$
k_{15}	$cat-n1 \rightarrow cat + n1$
k_{16}	$cat-n2 \rightarrow cat + n2$
k_{18}	$cat-n3 \rightarrow cat + n3$
k_{19}	$cat \rightarrow inact$

where Rh = rhodium precursor complex, cat = active catalyst, inact = inactive rhodium species, ol1 = octene-1, ol2 = internal octene isomers, sat = octane, n1 = *n*-nonanal, n2 = 2-methyl-octanal, and n3 = internal nonanal isomers.

In this simplified model, complex species such as cat–ol1, for example, represent kinetically necessary intermediates. Cat–ol1 represents an α-olefin complex or an alkyl complex produced by reversible insertion which can decompose to yield an α-olefin complex. Cat–n1 represents an intermediate which is committed to linear aldehyde formation. Cat–n2 represents an intermediate committed to the formation of the 2-methyl substituted aldehyde isomer. The nature of these intermediates, see Section 4, is

unclear, but their existence is kinetically necessary. A step such as cat–ol1 → cat–n1 (k_{11}) then represents the selectivity determining step on the path from an α-olefin to a linear aldehyde. Correspondingly, cat–ol1 → cat–n2 (k_{12}) is then the selectivity determining step on the path from the α-olefin to the 2-methyl substituted aldehyde isomer.

The ratio of the rate constants k_{11}/k_{12} was used to calculate energy differences. A comparison of ratios compensates for systematic errors. ΔE_A was determined at 100°C using $\Delta E_A = RT \ln(k_{11}/k_{12})$.

2.4. Method for obtaining crystals

Chelating ligand (0.5 mmol) was dissolved in 10 ml CH_2Cl_2 (dried over P_2O_5). 0.1 g $[RhCl(CO)_2]_2$ (0.25 mmol) was added at room temperature. The solution was stirred at RT 4.5 h until no further CO loss was observed. The solvent removed under vacuum and the residue recrystallized out of toluene (dried over Na) in an argon atmosphere.

2.5. Crystal structures

Crystals for X-ray analysis were coated with a perfluoropolyether oil, mounting at the end of a glass fiber and then placed in a N_2 cold-stream. Diffraction data were measured on a Nicolet P21 (ligand **1**) and Siemens P4 (ligand **2**) diffractometer with graphite monochromated Cu $K\alpha$ radiation using $\omega/2\theta$ scans. The structures were solved by Patterson (complex with ligand **1**) and direct (complex with ligand **2**) methods and refined using blocked full-matrix least-squares with anisotropic displacement parameters for all non-hydrogen atoms (SHELXTL-PLUS) [15]. Hydrogen atoms were refined with geometric constraints and isotropic displacement parameters. An empirical absorption correction was applied using the program DIFABS [16].

---

[3] A detailed description of the computational method can be found in Refs. [13,14]. The program used can be obtained from Project SERAPHIM, Department of Chemistry, University of Wisconsin-Madison, 1101 University Avenue, WI 53706: R.J., McKinney, F.J. Weigert, program number IB-1407,8.

2.6. Ligand *1*

$C_{57}H_{64}O_{11}P_2ClRh \cdot C_7H_8$, $M = 1217.5$, crystal dimensions $0.12 \times 0.17 \times 0.28$ mm^3, triclinic, $a = 11.192(4)$, $b = 14.444(4)$, $c = 19.206(6)$ Å, $\alpha = 100.30(2)$, $\beta = 91.37(3)$, $\gamma = 109.51(2)°$, $V = 2867.6$ Å^3, $T = 143$ K, $F(000) = 1272$, space group $P\bar{1}$, $Z = 2$, $D_c = 1.410$ g cm^{-3}, $\mu(Cu\ K\alpha) = 39.2$ cm^{-1}, 7643 reflections measured ($2\theta < 115°$) of which 6219 were observed ($|F_o| > 4\sigma|F_o|$). Final residuals were $R = 0.039$, $R_w = 0.037$, $w^{-1} = \sigma^2(F_o) + 3.6 \times 10^{-4}F_o^2$, maximum residual electron density $= 0.534$ eÅ^{-3}.

2.7. Ligand *3*

$C_{59}H_{64}O_{11}P_2ClRh \cdot 2(C_7H_8)$, $M = 1325.6$, crystal dimensions $0.25 \times 0.25 \times 0.30$ mm^3, monoclinic, $a = 15.528(3)$, $b = 15.805(3)$, $c = 29.582(6)$ Å, $\beta = 102.29(2)°$, $V = 6636.8$ Å^3, $T = 203$K, $F(000) = 2760$, space group $P2_1/n$, $Z = 4$, $D_c = 1.327$ g cm^{-3}, $\mu(Cu\ K\alpha) = 33.9$ cm^{-1}, 9673 reflections measured ($2\theta < 115°$) of which 8848 were unique and 5941 were observed ($|F_o| > 4\sigma|F_o|$). Final residuals were $R = 0.041$, $R_w = 0.045$, $w^{-1} = \sigma^2(F_o) + 1.9 \times 10^{-3}F_o^2$, maximum residual electron density $= 0.725$ eÅ^{-3}.

The crystal with ligand **1** was found to contain one molecule and that with ligand **3** two molecules of toluene in the crystallographic asymmetric unit. The structure analysis of (**1**) showed the crystal to contain two stereoisomers, in which the carbonyl and chloride ligands are interchanged with respect to the (asymmetric) phosphites, which show no disorder in the crystal lattice. The crystal used for the analysis showed a ca. 84:16 distribution of these stereoisomers and Fig. 4a shows the structure of the major isomer. However, it cannot be assumed that all crystals obtained from this preparation will exhibit the same ratio of stereoisomers. The structure was refined with a chloride and a carbonyl at both coordination positions (with occupancies of 0.84:0.16 and 0.16:0.84,

respectively). As a consequence, the Rh–C bond length appears considerably longer (2.02(1) Å) and the Rh–Cl a little shorter (2.35(1) Å) than the mean values seen for other crystal structures deposited in the Cambridge Crystallographic Database (viz. 1.82(5) and 2.40(4) Å, respectively). The crystal structure of (**3**) did not exhibit the presence of more than one stereoisomer (see Fig. 4b). However, it cannot be ruled out that small amounts of the other isomer are also present, or that another crystal contains the other, or a mixture of the two, stereoisomers.

Further details of the crystal structure determinations are available on request from the Fachinformationszentrum Karlsruhe, Gesellschaft für wissenschaftlich-technische Information, D-76344 Eggenstein-Leopoldshafen, quoting the deposition numbers CSD-102889, CSD-102890, the names of the authors, and the journal citation.

2.8. Molecular modeling

All calculations were done using the CHARMm21 forcefield as implemented in Quanta (Molecular Simulations, 9685 Scranton Road, San Diego, CA 92121, USA) on a Silicon Graphics Indigo2 workstation. No special geometry was assumed around the rhodium atom: The chelating phosphite ligand and the *n*-octyl (or *i*-octyl) ligand were bound to the metal. Bond stretching terms from the metal to the attached atoms was defined based on crystallographic values and the angle and torsional terms were set to zero. Non-bonded terms (Lennard-Jones 6–12) were set by the parameter chooser in Quanta.

Charges were assigned using the tools in Quanta and were averaged to total charge of zero for all structures. All degrees of freedom were varied during minimization to allow the *n*- and *i*-alkyl adducts to attain the optimal geometries. Minimization was carried out with the Adopted-Basis-Newton–Raphson (ABNR) minimizer with an energy gradient tolerance of 0.001 kcal.

Conformational searching was done using the random search method where all nonterminal torsions were varied. Ring torsions were varied as well and a ring closure bond (elastic bond) was defined to explore the complete torsional space of the molecule. The torsional angle window was 180°. Each conformation was minimized and used as the starting point for the next conformation. One hundred fifty conformations per molecule were generated. As a test of completeness of the conformational search protocol a representative molecule was chosen and 500 conformations were generated. No low-energy conformations were found in addition to those generated in the 150 conformer search. The global energy minima and all conformations within 10 kcal of it were kept for further analysis.

The *n*- and *i*-alkyl ligands were added onto the rhodium complex and a conformational search of the alkyl ligand was carried out while the rhodium complex was held fixed. The global energy minima for the *n*- and *i*-alkyl adduct were then minimized with all structural parameters free to vary. The total energy difference between the *n*- and *i*-alkyl was computed and used in comparison to the relative energies in kinetic model.

3. Results

Sterically hindered chelating phosphite ligands were first described in patents from Union Carbide [7]. As is usual in such systems, small changes in the ligand structure cause large differences in the observed catalyst selectivities. In particular, the product linearity, defined as the ratio of linear aldehyde to total aldehyde produced, is extremely sensitive to structural changes. We wished to develop a structure–activity relationship in order to quickly and efficiently investigate and understand these systems.

A simplified kinetic model (Fig. 2) for the low-pressure rhodium catalyzed hydroformylation of α-olefins was used in order to quickly quantify catalyst properties in solution. This approach allows the treatment of very complex systems (in this case multiple parallel reactions) using PC software and easily obtainable analytical data (such as GC data).
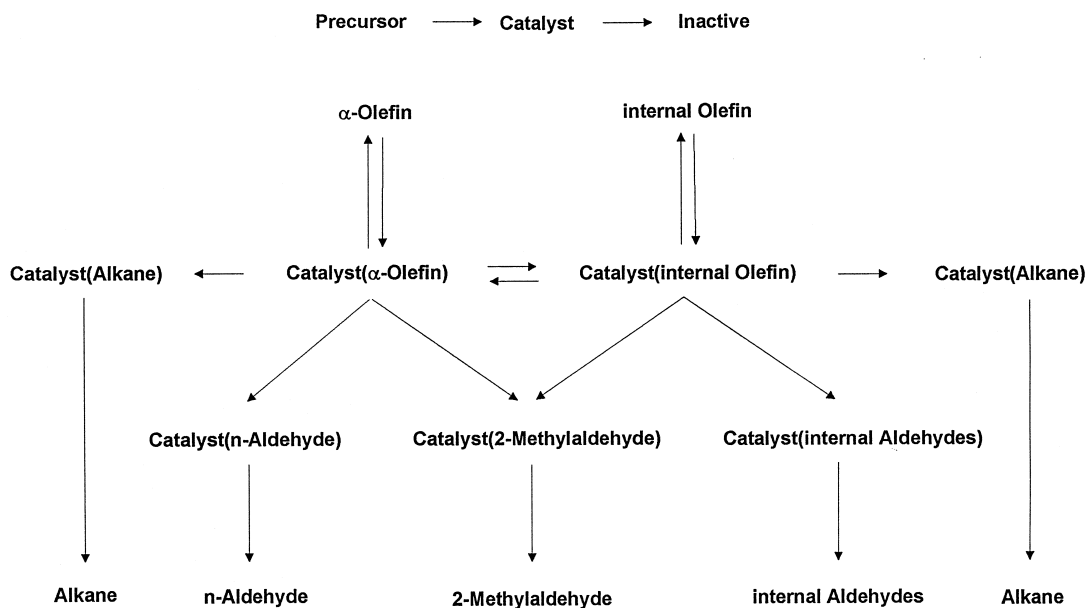

Fig. 2. Kinetic model for the low-pressure rhodium catalyzed hydroformylation of α-olefins.

The main assumption in this model is that all of the chemical steps occur on the same catalyst center. This assumption is of course only valid for chelating ligand systems where the changes in phosphorus ligand coordination number and the structural isomerism known for monodentate ligands [17] are severely restricted. It was also assumed that CO and H_2 are present in excess. And it was assumed that, to a first approximation, all internal olefins react similarly.

The first step is a reversible binding of either an α- or internal olefin. A bound olefin can be isomerised, hydrogenated or hydroformylated. A linear aldehyde or an aldehyde with a 2-methyl substituent can be formed from an α-olefin. A 2-methyl-substituted or 2-ethyl-substituted aldehyde can be formed from an olefin with the double bond in the 2 position. The 2-ethyl-substituted aldehyde and the higher 2-alkyl-substituted aldehydes which are formed from other internal olefins are handled together in order to simplify the model. The products must

be released from the catalyst center. Finally, a point which is often ignored, although catalyst precursors are usually used, the active catalyst must first be formed and can deactivate during the observed reaction time. All of these steps are approximated with first-order rate constants and varied using a multiparameter Gear iterator until the best fit is achieved.
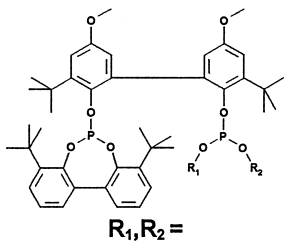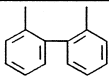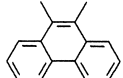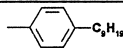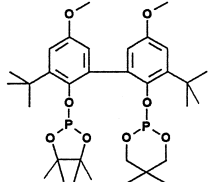
Kinetic experiments were carried out under standard conditions and the rate constants in the model shown in Fig. 2 were varied as describe above until the best fit was achieved (see Section 2). The fit to data obtained using ligand **1** and ligand **2** is shown in Fig. 3. The symbols are experimental data points and the curves are calculated. The human eye remains one of the best instruments for determining the goodness of the fit. One can see that this model fits quite well. Significant changes in the assumptions in the model above lead to significant deviations in the calculated curves. Most importantly, the model discussed above is the simplest model
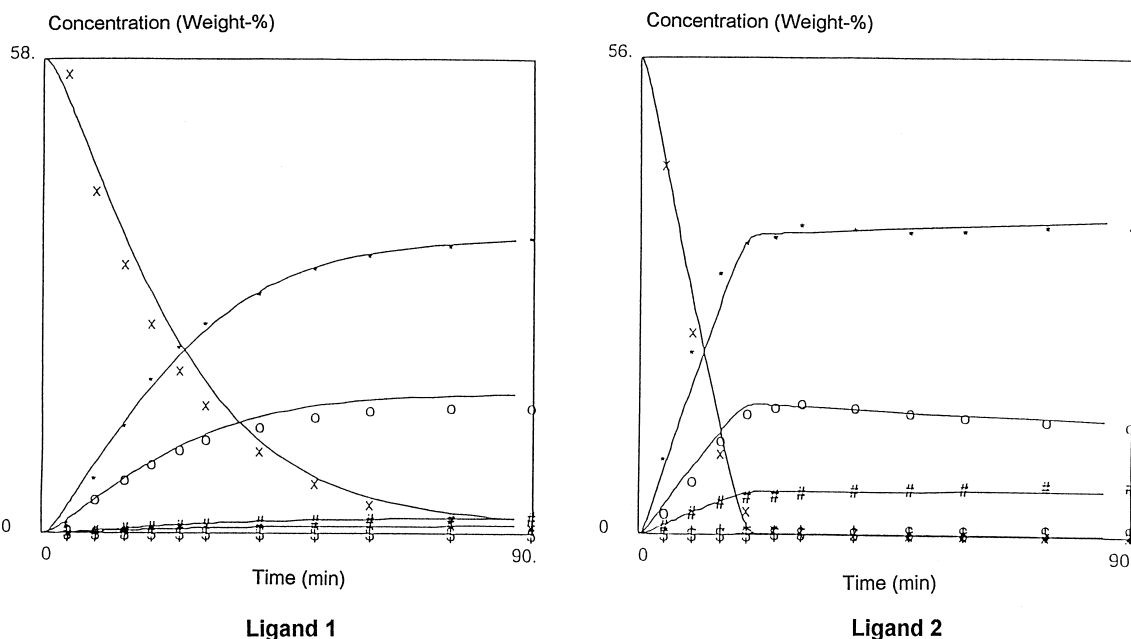
X = 1-octene; o = internal octene isomers; + = octane; * = n-nonanal; # = 2-methyloctanal; $ = internal nonanal isomers

Fig. 3. GIT-output: experimental (points) and calculated (continuous lines) kinetic data (L/Rh = 5, 1-octene, 100°C, 10 bar CO/H_2 (1:1)) for ligand **1** and ligand **2**.

Table 1
Experimental data and molecular modeling results for selected ligands

Ligand #	R₁,R₂ =	Kinetic Data			Molecular Modelling
		Product Linearity %	k_n / k_{iso}	ΔE_A kcal/mol	ΔE_{Tot} kcal/mol
1		95.7	22.2	2.30	32.2
2		87.9	7.2	1.47	29.75
3		84.2	5.3	1.24	29
4	—⟨⟩—C₉H₁₉	92.5	12.4	1.86	31.5
5		89.3	8.4	1.58	30.4

[Ligand 1]Rh(CO)Cl   [Ligand 3]Rh(CO)Cl
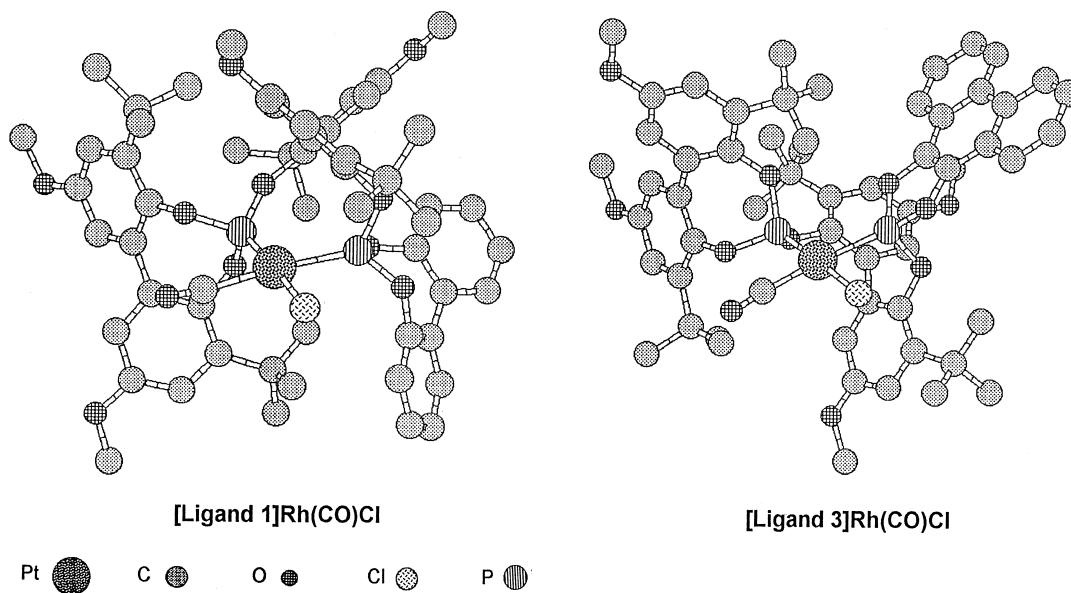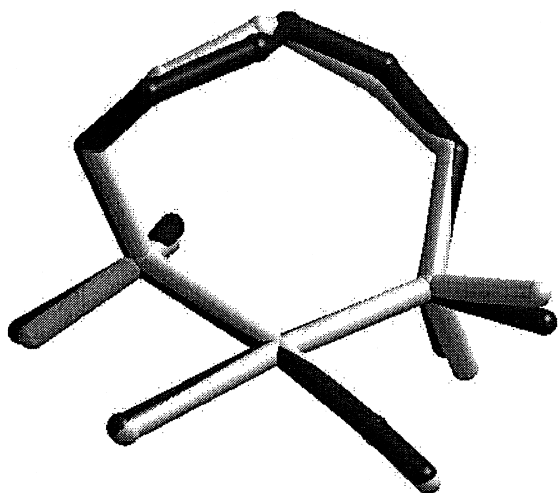
Pt ⬤   C ◉   O ◉   Cl ◎   P ◍

Fig. 4. X-ray structures [Ligand]Rh(CO)Cl for ligands **1** and **3**.

Light: crystal structure [Ligand 1]Rh(CO)Cl
Dark: crystal structure [Ligand 3]Rh(CO)Cl

Fig. 5. Overlapping core regions from X-ray structures.

found which adequately describes the experimental data.

This methodology allows a quick quantitative comparison of the rate constants for the formation of linear and 2-methyl-substituted aldehydes from α-olefins. The ratio of these rate constants is determined by the energy difference in the (at this point unknown, see Section 4 for

mechanistic alternatives) selectivity-determining step of the catalytic cycle. Approximate energy differences for selected ligands are listed in Table 1.

Molecular modeling is a suitable method for quantifying the differences in the structures of metal–ligand complexes. A preliminary comparison with X-ray data was, however, necessary in order to test the validity of the modeling results. In order to accomplish this, single crystal X-ray structures (Fig. 4) of the easily obtainable carbonyl chloride complexes [Ligand]Rh-(CO)(Cl) were obtained for ligand **1** and ligand **3**. A comparison of the core regions of these complexes (Fig. 5) indicates that the important distances and angles are relatively constant from structure to structure.

Molecular modeling (see Section 2) of these complexes yields quite similar structures, when crystal packing effects are taken into account. This can most easily be seen by superimposing the X-ray structures and the structures obtained by molecular modeling (Fig. 6). One sees, for example, that the low energy conformations of the complex with ligand **1** have a different orientation of the unsubstituted nonbridging biphenyl group. An examination of the crystal

[Ligand 1]Rh(CO)Cl   [Ligand 3]Rh(CO)Cl
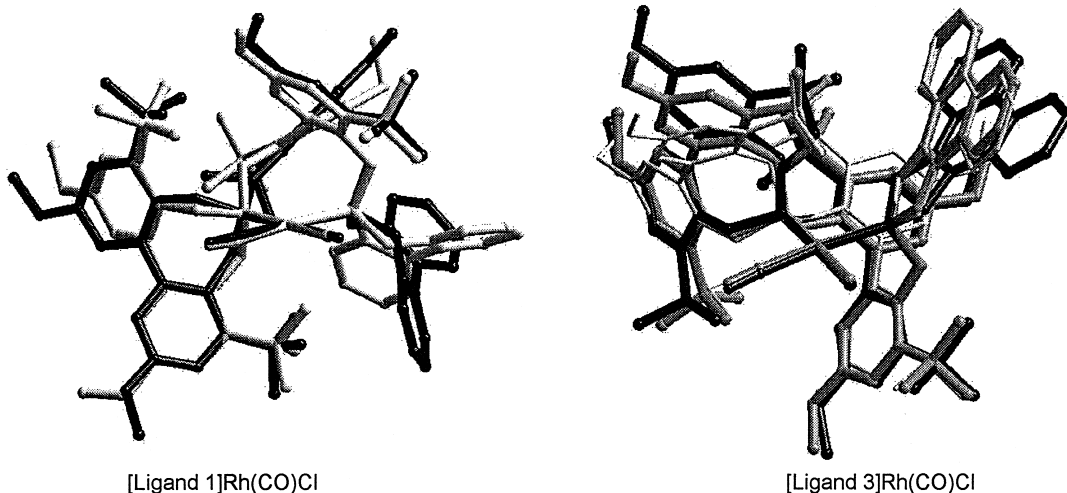
Core region: molecular modeling thick light; crystal structure thick dark; optimized crystal structure (Ligand 3) thin

Fig. 6. Comparison of single crystal X-ray data with structures obtained via molecular modeling.
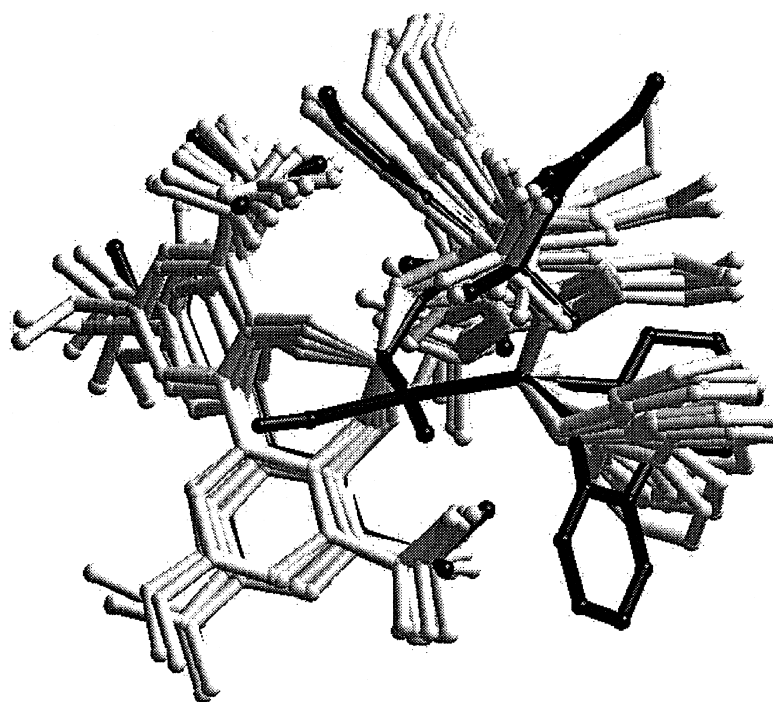
Dark: lowest energy structure; Light: energetically accessible structures

Fig. 7. Superimposition of the low-energy structures obtained for Rh/ligand **1** (up to +5 kcal/mol).

structure, however, leads to the conclusion that this can be accounted for by crystal packing effects and is not an artifact of the forcefield. A comparison of the X-ray crystal structure (dark) of ligand **3** to the lowest energy conformation determined by molecular modeling (light) also shows large differences, particularly in the phenanthrenyl group. These can, however, also be ascribed in part to crystal packing effects, as well as the functional form of the forcefield. If the crystal structure is optimized (thin stick) the agreement with the lowest energy conformation
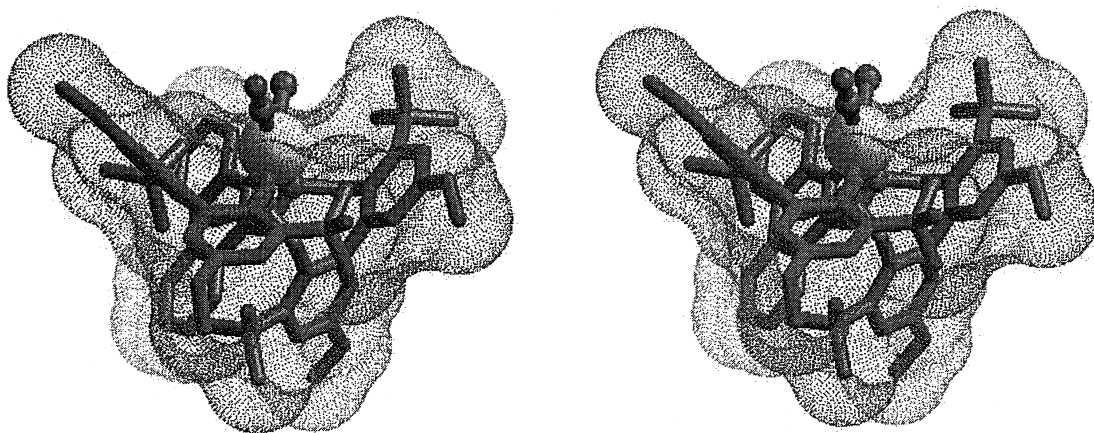

Fig. 8. Accessible surface of [Ligand **1**]Rh(CO)(Cl) (1.4 Å probe).

is much better. It is important to note here that it is the similarity between the energy-minimized crystal structure and the low-energy conformations of the modeling that is important when using modeling as a predictive tool.

Interestingly, a consideration of the structures with up to 5 kcal/mol additional energy obtained via molecular modeling for the complex with ligand **1** suggests that the complexes are relatively rigid. This can be most easily seen by superimposing these structures and observing the relative structural changes (Fig. 7). One can see that the variation is not large.

A consideration of the accessible surface (1.4 Å Probe, Fig. 8) of, for example, [ligand **1**]Rh(CO)(Cl) is also very informative. The chelating ligand wraps itself around the metal center in such a manner that an asymmetric enzyme-like pocket is formed.

Extensive investigations of homogeneous hydrogenations in the literature [18] suggest that the interactions between the substituents at the free rhodium coordination sites and regions of the ligand inside this pocket determine the course of the chemistry at these sites. Such interactions were investigated for the complexes studied here with the help of molecular modeling using linear and branched alkyl groups as 'molecular probes'. [4] A particular geometry for the selectivity determining intermediates was not assumed (see Section 2). [5] The energy of the rhodium complex was obtained using linear (*n*-octyl) and 2-methyl branched (*i*-octyl) alkyl
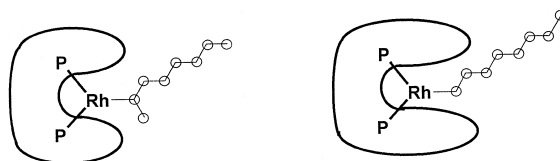

Fig. 9. Interaction of linear and branched alkyl groups with the inner surface ('pocket') of a rhodium complex with a chelating phosphite ligand.

groups for each ligand studied. This is schematically shown in Fig. 9. The relative energy differences ΔE_{Tot} for the lowest energy conformations of selected complexes are given in Table 1.

The energy differences obtained with molecular modeling for the interactions of such linear and 2-methyl branched alkyl groups with the ligand pocket were plotted against the energy differences in the selectivity determining step obtained from the kinetic experiments for each ligand. A linear correlation was found, as can be seen in Fig. 10.

4. Discussion

The correlation observed above demonstrates that the simple steric interactions measured using molecular mechanics induce significant differences in the observed product linearities. The question, however, is: why does this simple correlation function so well? One is led to consider which step in the catalyst cycle actually determines the observed selectivity.

The key finding that ligands which stabilize a P–Rh–P angle of approximately 120° lead to highly selective catalysts for the low pressure rhodium catalyzed hydroformylation has been extensively discussed in the literature [4,6,11]. Stabilization of a trigonal bipyramidal intermediate [17] with two equatorially coordinated phosphorus centers is postulated [20]. [6] The

---

[4] An alternative molecular modeling approach is to define the accessible molecular surface (AMS) of a rhodium center within a flexible [(P$_2$)Rh] fragment. Molecular mechanics are used here to explore the conformation space inside the cavity and a 'pseudo-solvent-accessible' surface is determined using a 1.4 Å probe [19]. An approach using alkyl groups as probes explores the 'substituent-accessible' surface. Initial efforts to correlate results obtained with an AMS-like approach with the kinetic results obtained using sterically hindered chelating phosphites were not successful.

[5] Molecular modeling studies in Hoechst are described in German Patent 4426577. A square planar structure was assumed and the energy differences for complexes with linear and branched alkyl groups bound to rhodium determined.

---

[6] Interestingly, in the case of asymmetric catalysis using chiral phosphine–phosphite ligands trigonal bipyramidal complexes are also formed. However, the ligand binds to equatorial and axial positions and favors a 90° bond angle.
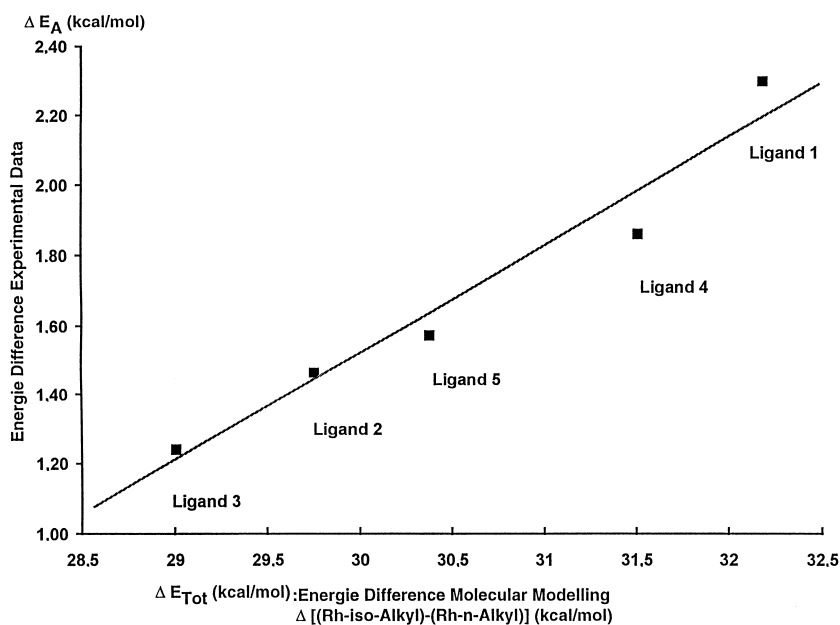
Fig. 10. Plot of the energy differences obtained via molecular modeling against the energy differences obtained from kinetic experiments.

chelating phosphite ligands investigated here all lead to highly active and selective catalysts with similar structures. By definition, the right complexes are formed at the right times using these ligands.

In Wilkinson's generally accepted dissociative mechanism [21–23], the regiochemistry of the hydroformylation is determined in the step where a trigonal bipyramidal olefin hydride complex is converted into square planar *n*- and
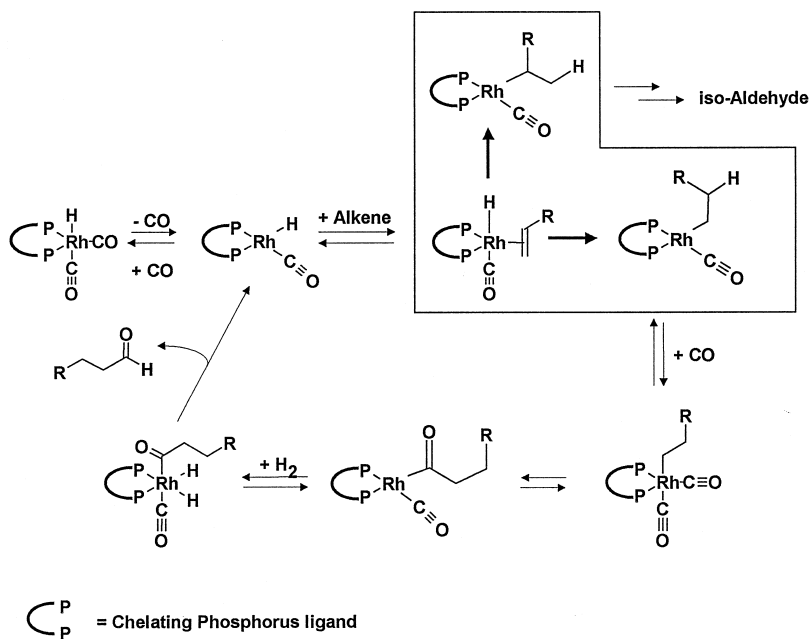

Fig. 11. Mechanism with irreversible olefin insertion (Wilkinson mechanism).

i-alkyl complexes (Fig. 11). This insertion has been postulated to be irreversible and therefore to determine the observed product ratios. This type of mechanism would be directly sensitive to the types of steric interactions measured using molecular mechanics.

Newer results in the literature concerning the origin of regioselectivity in the hydroformylation, however, are somewhat contradictory. Magnetization transfer studies using 3,3-dimethyl-1-butene in the presence of a rhodium bisphosphite hydride complex in the absence of CO suggest that although a rapid, reversible alkene insertion occurs in solution, the observed regiochemistry during hydroformylations is not determined by this step or any step prior to it (Fig. 12) [24]. It should be noted, however, that the NMR experiments were made under mass transfer limited conditions which favor alkene isomerisation. Despite this limitation, these data imply that the interactions measured using molecular mechanics in this study are only an indirect indicator of the energy differences in, for example, intermediates such as acyl complexes.

In contrast, deuteroformylation of 1-hexene with a rhodium–bisphosphine complexes shows that the regiochemistry of aldehyde is set by a largely irreversible insertion of the alkene in the rhodium hydride to produce a rhodium alkyl
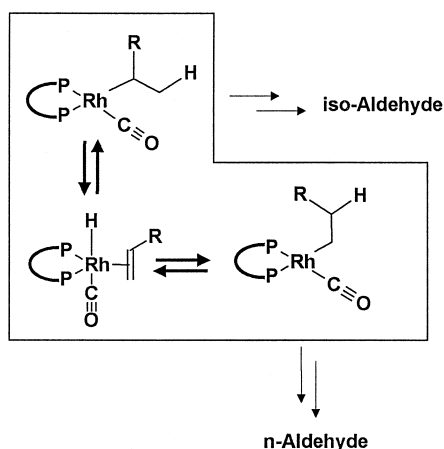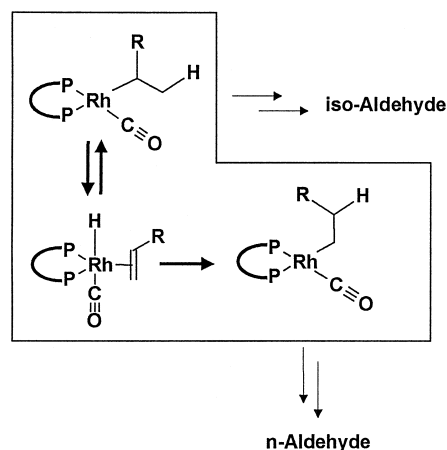

Fig. 13. Mechanism with partially reversible olefin insertion.

committed to aldehyde formation. Interestingly, although the linear alkyl group almost exclusively yields aldehyde, the branched alkyl group reverts 75% of the time to bound olefin (Fig. 13) [25,26]. This type of mechanism, which was also seen in deuterioformylation of 1-hexene using $Rh_4(CO)_{12}$ [27], would also be directly sensitive to the types of steric interactions measured using molecular mechanics.

It should be noted that these studies were carried out at relatively mild temperatures (32°C). Deuterioformylations of 1-hexene at higher temperatures (80°–100°C) with Rh_4-$(CO)_{12}$ have shown that the olefin insertion reactions become more reversible under these conditions [27].

The kinetic studies reported here were carried at 100°C and in a well-stirred autoclave without mass transfer limitations. Under these conditions, the formation of internal olefins was considerably slower than observed in the NMR studies (see data, Fig. 3). A mechanism with irreversible olefin insertion (Fig. 11), however, seems unlikely at these temperatures. A mechanism where the regioselectivity is determined in a later step in the catalytic cycle, as in the previously reported NMR studies with chelating phosphites, also seems unlikely in the presence of significant amounts of CO but cannot be ruled out. A partially reversible olefin insertion,

Fig. 12. Mechanism with fully reversible olefin insertion.

i.e., where the *n*-alkyl is predominantly and irreversibly trapped by CO and the *i*-alkyl largely reverts back to the olefin complex (Fig. 13) would seem to be most likely in light of the present literature. This type of mechanism would also be directly sensitive to the types of steric interactions measured using molecular mechanics. Further detailed studies, for example deuterioformylations with chelating phosphite ligands, are, however, necessary in order to more precisely understand the origin of the observed steric effects.

5. Conclusion

The structure–activity relationship outlined in this paper can be used in order to quickly optimize the structurally similar catalysts obtained with chelating ligands [28]. This method, however, requires a known ligand which yields active and selective catalysts as its starting point and electronic factors are not treated. Other methods, such as the measurement of 'natural bite angles', also treat the electronic problem indirectly by seeking ligands which stabilize particular structures such as trigonal bipyramidal rhodium complexes. We are currently developing embedding methods, which allow an ab initio quantum mechanical treatment of the catalytic core and simultaneous molecular mechanics treatment of the ligand periphery. This strategy should provide a method which accurately treats both steric and electronic effects simultaneously and at reasonable computational costs.

References

[1] K. Weissermel, H.-J. Arpe, Industrielle Organische Chemie, 4th edn., VCH Verlagsgesellschaft, Weinheim, Germany, 1994.

[2] M. Beller, B. Cornils, C.D. Frohning, C.W. Kohlpaintner, J. Mol. Catal. A 104 (1995) 17–85.

[3] T.J. Devon, G.W. Phillips, T.A. Puckette, J.L. Stavinoha, J.J. Vanderbilt, US Patent 4,694,109 (to Eastman Kodak).

[4] C.P. Casey, G.T. Whiteker, M.G. Melville, L.M. Petrovich, J.A. Gavney Jr., D.R. Powell, J. Am. Chem. Soc. 114 (1992) 5535–5543.

[5] W.A. Herrmann, C.W. Kohlpaintner, H. Bahrmann, W. Konkol, J. Mol. Catal. 73 (1992) 191–201.

[6] M. Kranenburg, Y.E.M. van der Burgt, P.C.J. Kamer, P.W.N.M. van Leeuwen, K. Goubitz, J. Fraanje, Organometallics 14 (1995) 3081–3089.

[7] E. Billig, A.G. Abatjoglou, D.R. Bryant, US Patent 4,769,498 (to Union Carbide).

[8] G.D. Cuny, S.L. Buchwald, J. Am. Chem. Soc. 115 (1992) 2066–2068.

[9] A. van Rooy, P.C.J. Kamer, P.W.N.M. van Leeuwen, N. Veldman, A.L. Spek, J. Organomet. Chem. 494 (1995) C15–C18.

[10] A. van Rooy, P.C.J. Kamer, P.W.N.M. van Leeuwen, K. Goubitz, J. Fraanje, N. Veldman, A.L. Spek, Organometallics 15 (1996) 835–847.

[11] A. van Rooy, P.C.J. Kamer, P.W.N.M. van Leeuwen, J. Organomet. Chem. 535 (1997) 201–207.

[12] P. Lorz, W. Bertleff, M. Roeper, D. Koeffer, Eur. Pat. 472071 (to BASF).

[13] R.N. Stabler, J. Chesick, Int. J. Kinet. 10 (1978) 461.

[14] F. Weigert, Comput. Chem. 11 (1987) 273–280.

[15] G.M. Sheldrick, SHELXTL-PLUS Manual, Siemens Analyt. X-ray Instr., Madison, USA, 1990.

[16] N. Walker, D. Stuart, Acta Crystallogr. A 39 (1983) 158–166.

[17] J.M. Brown, A.G. Kent, J. Chem. Soc. Perkin Trans. 2 (1987) 1597–1607.

[18] B. Bosnich (Ed.), Asymmetric Catalysis, Martinus Nijhoff, Dordrecht, 1986.

[19] K. Angermund, W. Baumann, E. Dinjus, R. Fornika, H. Goerls, M. Kessler, C. Krueger, W. Leitner, F. Lutz, Chem. Eur. J. 3 (5) (1997) 755–764.

[20] K. Nozaki, N. Sakai, T. Nanno, T. Higashijima, S. Mano, T. Horiuchi, H. Takaya, J. Am. Chem. Soc. 119 (1997) 4413–4423.

[21] D. Evans, J.A. Osborn, G. Wilkinson, J. Chem. Soc. A (1968) 3133–3142.

[22] G. Yapgupsky, C.K. Brown, G. Wilkinson, J. Chem. Soc. A (1970) 1392–1401.

[23] C.K. Brown, G. Wilkinson, J. Chem. Soc. A (1970) 2753–2764.

[24] B. Moasser, W.L. Gladfelter, D. C. Roe, Organometallics 14 (1995) 3832–3838.

[25] C.P. Casey, L.M. Petrovich, J. Am. Chem. Soc. 117 (1995) 6007–6014.

[26] C. Bianchini, L. Glendenning, Chemtracts–Inorg. Chem. 7 (1995) 116–119.

[27] R. Lazzaroni, G. Uccello-Barretta, M. Benetti, Organometallics 8 (1989) 2323–2327.

[28] R. Paciello, L. Siggel, M. Röper, manuscript in preparation.